

Numerical Simulation and Experimental Validation of a Flux Switching Permanent Magnet Memory Machine

ZHONGXIAN CHEN^{1,2} AND YINGJIE CUI¹

¹School of Intelligence Manufacturing, Huanghuai University, Zhumadian 463000, China

²Henan Key Laboratory of Smart Lighting, Huanghuai University, Zhumadian 463000, China

Corresponding author: Zhongxian Chen (zhongxian1984@163.com)

This work was supported by the Key Scientific Research Projects of Higher Education Institutions in Henan Province under Grant 2017-302.

ABSTRACT Compared with the traditional flux switching permanent magnet machine, flux switching permanent magnet memory (FSPMM) machine has two kinds of permanent magnets, flux regulating windings and complex flux path. In this article, a three phase FSPMM machine with 12 stator slots and 14 rotor poles is optimized by numerical simulation software. After the pole-arc optimization, there is only one suitable skewed slot degree of rotor that can further increase the sinusoidal degree of back electromotive-force (EMF) of FSPMM machine, and decreases the amplitude of EMF slightly. Besides, the flux regulating of FSPMM machine includes enhance flux is analyzed by numerical simulation software. Lastly, a prototype of FSPMM machine is constructed, and the obtained numerical simulation results are verified by experimental tests. The simulation and experimental results may be benefit for the research of operational control, flux regulation and industry application of FSPMM machine in future.


INDEX TERMS Flux switching, flux regulating, skewed slot, back electromotive force.

I. INTRODUCTION

Flux switching permanent magnet memory (FSPMM) machine is a novel flux switching permanent magnet machine that has the function of flux regulating, including the enhance flux and weaken flux [1]–[3]. Different from the traditional online flux regulating by continuous current, the flux regulating of FSPMM machine can be realized by injecting one pulse current (usually less than 1ms) into flux regulating windings, which aim is to change the work point of low-coercive-force permanent magnet materials [4], [5].

After the work point changing of low-coercive-force permanent magnet materials, the air-gap flux density of FSPMM machine can be weakened or enhanced, thus the amplitude of back electromotive-force (EMF) waveform, speed, torque density and cogging force can be also changed. In this situation, the FSPMM machine is suitable for the domain of wide speed range and variable torque such as electric vehicle, aeronautics and astronautics, etc [6]–[9].

Actually, the speed range, torque density and cogging force of FSPMM machine can be reflected by the back EMF waveform [10]–[12]. For example, the amplitude variation

The associate editor coordinating the review of this manuscript and approving it for publication was Feifei Bu .

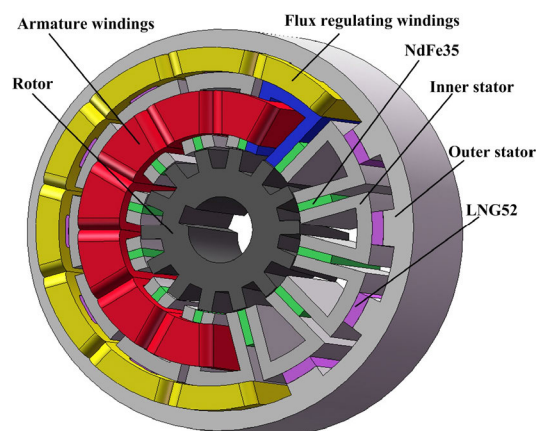


FIGURE 1. The three-dimensional structure of FSPMM machine.

range of back EMF waveform decides the speed range and torque density, and the more sinusoidal degree of back EMF waveform, the smaller cogging force. Therefore, some papers concentrate on the back EMF waveform performance of FSPMM machine.

In order to investigate the amplitudes of back EMF waveforms, E-core topology and C-core topology of switch flux hybrid magnet memory (SFHMM) machine are

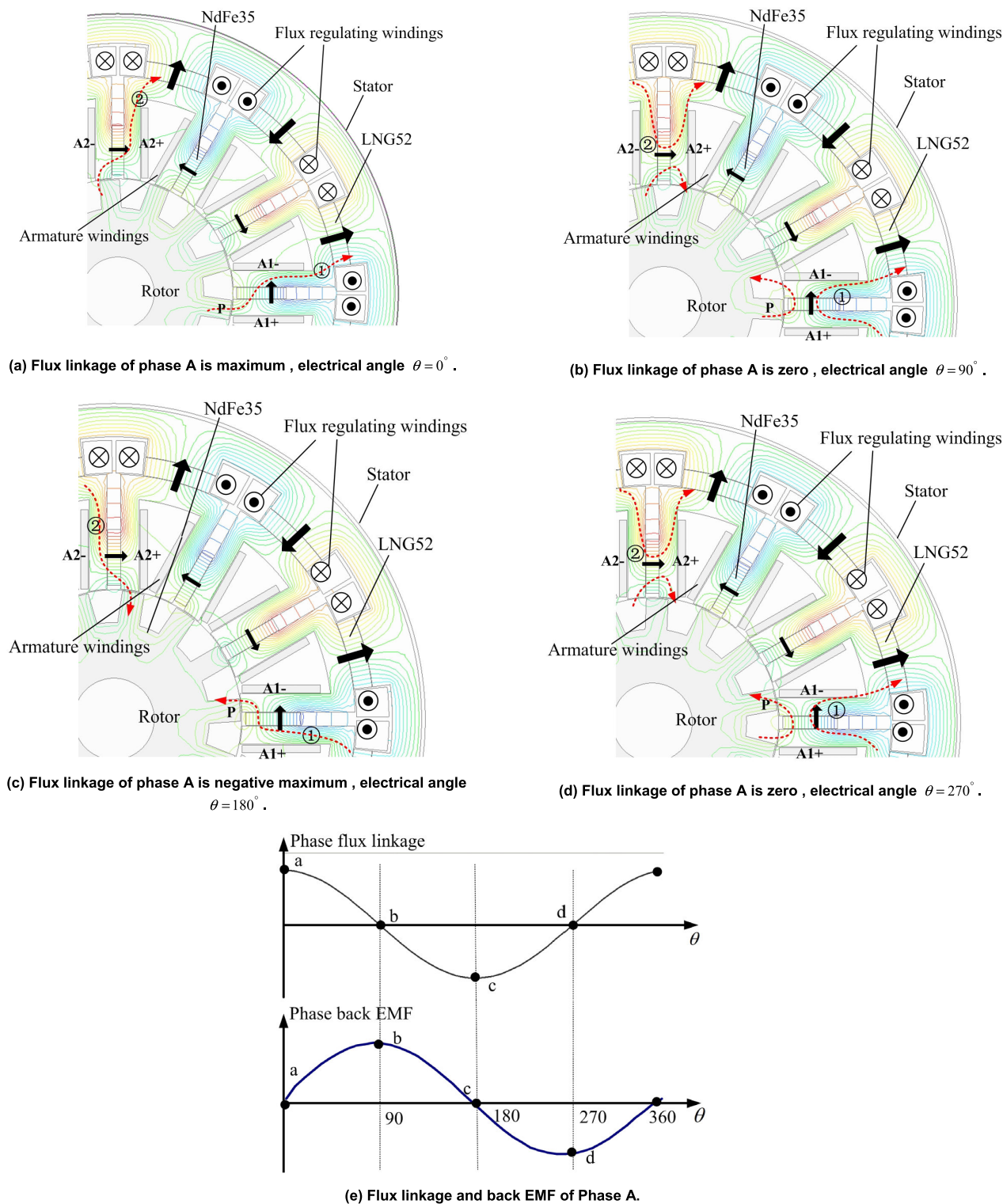


FIGURE 2. The flux switching principle and back EMF waveform of FSPMM machine.

analyzed [13]. Besides, the sinusoidal degree of back EMF waveforms of traditional flux switch permanent magnet machines are optimized by pole-arc [14], [15], axial magnetization and halbach permanent magnet arrays [16]–[18].

However, the above papers are generally put the focus on the stator structure design, magnetization direction

optimization and general design method. Therefore, this article investigates the back EMF waveforms performance of FSPMM machine by rotor structure improvement, includes the harmonics analysis, weakened flux and enhance flux.

In this article, the back EMF waveform of FSPMM machine is optimized by pole-arc and skewed slot type rotor.

Based on the pole-arc optimization, the numerical simulation results indicate that the sinusoidal degree of back EMF waveform can be further improved by the skewed slot type rotor. Besides, the harmonics of back EMF waveforms of FSPMM machine with enhance flux and weaken flux are analyzed. Then, a three phase FSPMM machine with 12 stator slots and 14 rotor poles is constructed, and the numerical simulation and optimization results are verified by the experimental tests.

II. STRUCTURE AND OPERATION PRINCIPLE OF FSPMM MACHINE

A. STRUCTURE

The three-dimensional structure of FSPMM machine with 12 stator slots and 14 rotor poles is shown in Fig. 1. Different from the traditional flux switching permanent magnet (FSPM) machine [19], the FSPMM machine has the second kind of permanent magnet LNG52, which is installed in the outside of stator and surrounded by field regulating windings. During the operation process, the permanent magnet NdFe35 contributes the main flux switch of air-gap flux density of FSPMM machine, and the permanent magnet LNG52 serves as the auxiliary function to weaken or enhance the air-gap flux density of FSPMM machine. Therefore, some paper named the FSPMM machine as hybrid permanent magnet machine (motor). Compared with the permanent magnet NdFe35, the permanent magnet LNG52 has the characteristics of low-coercive-force, which can be magnetized or demagnetized by the pulse current of field regulating windings. The magnetization and demagnetization of LNG52 are the key to achieve the memory function of FSPMM machine, and will be elaborated in the C part of this Section.

B. OPERATION PRINCIPLE

Based on the numerical simulation software, Fig. 2 shows the flux switching principle of FSPMM machine (1/4 part). In Fig. 2(a) ~ Fig. 2(d), the red arrows indicate the flux path near phase A1 and A2, which can increase or decrease the back EMF amplitude of phase A during the rotor motion. The stator is static, and the rotor rotates along the inner diameter of stator, which results the flux switching between stator and rotor. Fig. 2(e) illustrates one period of phase flux linkage and phase back EMF by electrical angle. When the P tooth of rotor is positioned near the A1 winding as shown in Fig. 2(a), the flux linkage of A1 and A2 is maximum. Due to the circular symmetry, the total flux linkage of phase A of FSPMM machine is also maximum, which corresponds to the electrical angle $\theta = 0^\circ$ in Fig. 2(e). Rotates the rotor anticlockwise to the relative position between rotate and stator as shown in Fig. 2(b), results the zero flux linkage of A1 and A2, thus the total flux linkage of phase A of FSPMM machine is zero, this means the electrical angle $\theta = 90^\circ$. When the relative position between stator and rotor is corresponds to the Fig. 2(c), it can be seen that the total flux linkage of phase A of FSPMM machine is negative maximum and the electrical angle $\theta = 180^\circ$. Fig. 2(d) indicates the total flux linkage of

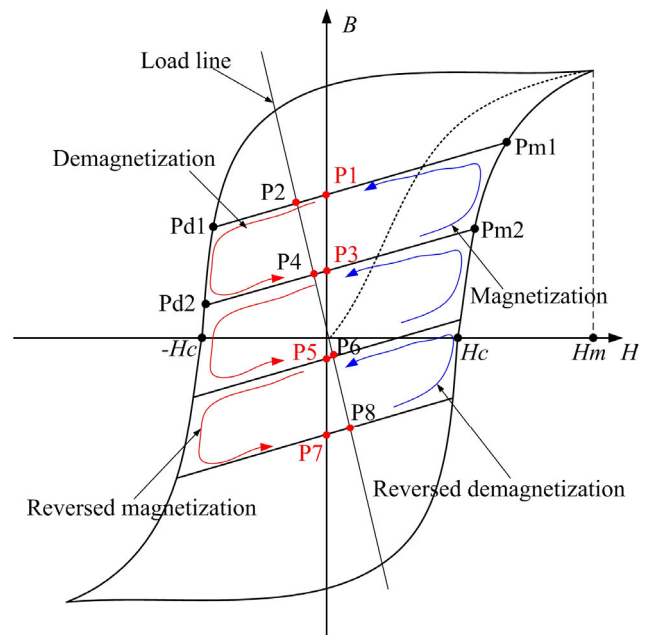


FIGURE 3. Magnetization and demagnetization of LNG52.

phase A of FSPMM machine is zero and the electrical angle $\theta = 270^\circ$.

By the differential calculation of phase flux linkage, the phase back EMF can be achieved. Therefore, Fig. 2(e) also shows the phase back EMF waveform of FSPMM machine. In Fig. 2(e), the electrical angle $\theta = 0^\circ$, $\theta = 90^\circ$, $\theta = 180^\circ$ and $\theta = 270^\circ$ are corresponding to the Fig. 2(a), Fig. 2(b), Fig. 2(c) and Fig. 2(d) respectively.

Besides, if the work point of low-coercive-force permanent magnet LNG52 is magnetized or demagnetized by flux regulating windings, then the amplitude of flux linkage and back EMF waveform is changed, which achieve the weaken flux and enhance flux of FSPMM machine. In the following C part, the magnetization and demagnetization principles of low-coercive-force permanent magnet LNG52 will be elaborated.

C. MAGNETIZATION AND DEMAGNETIZATION PRINCIPLES OF PERMANENT MAGNET LNG52

The coercive force of LNG52 is about 56kA/m, which is much lower than the coercive force of NdFe35 (625kA/m). Therefore, without impacts on the NdFe35, it is possible to change the work point of low-coercive-force permanent magnet LNG52 by the suitable pulse current of flux regulating windings. Fig. 3 shows the magnetization and demagnetization principles of LNG52. In Fig. 3, H_c is the coercive force, H_m is the maximum magnetic field and B is the magnetic flux density. For example, by a suitable amplitude of pulse current of flux regulating windings, a demagnetization magnetic field is occurs and passes though the LNG52, and the no-load work point of LNG52 can be shifted from P1 to P3 though Pd1 and Pd2. If it is in load condition, the load work point of LNG52 can be moved from P2 to P4 though Pd1 and Pd2. On the other hand, if an opposite pulse current

injects into the flux regulating windings, the no-load point of LNG52 can be moved from P3 to P1 though Pm2 and Pm1 (or moved from P4 to P2 though Pm2 and Pm1, in the load condition).

Besides, the reversed demagnetization and magnetization of LNG52 are similar to the above analysis process, which occur in the third and fourth quadrant of Fig. 3. Therefore, combines with the structure of FSPMM machine (Fig. 2), it can be known that demagnetization and magnetization of LNG52 can change air-gap flux density of FSPMM machine, which will be analyzed and optimized in the following.

III. OPTIMIZATION OF FSPMM MACHINE

For the traditional flux switching permanent magnet machine, some paper proposed the method of rotor pole-arc optimization to decrease the harmonic content of back EMF waveform. However, the harmonic content can be further decreased by the method of skewed slot of rotor.

In order to ensure the width of stator tooth and rotor tooth (avoids the magnetic saturation occurs in stator tooth and rotor tooth), we optimal the back EMF waveform of FSPMM machine by pole-arc coefficient preliminary, and then increase the sinusoidal degree of back EMF waveform further by skewed slot of rotor.

A. POLE-ARC AND SKEWED SLOT OPTIMIZATION

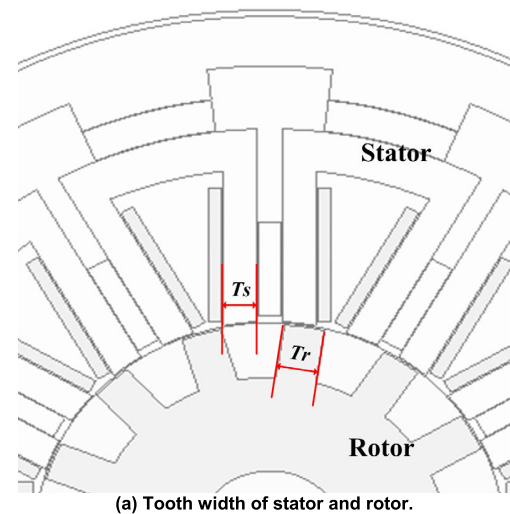
For the FSPMM machine, the larger stator tooth width will limit the size of permanent magnet and the number of armature windings, or the smaller stator tooth width will improve the magnetic saturation of stator tooth. Therefore, the stator tooth width is designed as $T_s = 8.22^\circ$, which is approximately equal to 1/4 polar distance of 12 stator slots of FSPMM machine, as shown in Fig. 4(a). In this precondition, the rotor tooth width T_r will has a great effect on the sinusoidal degree of back EMF waveform. The detailed analysis process can be referenced by [19].

It is assumed that the relationship between rotor tooth width T_r and stator tooth width T_s can be expressed as

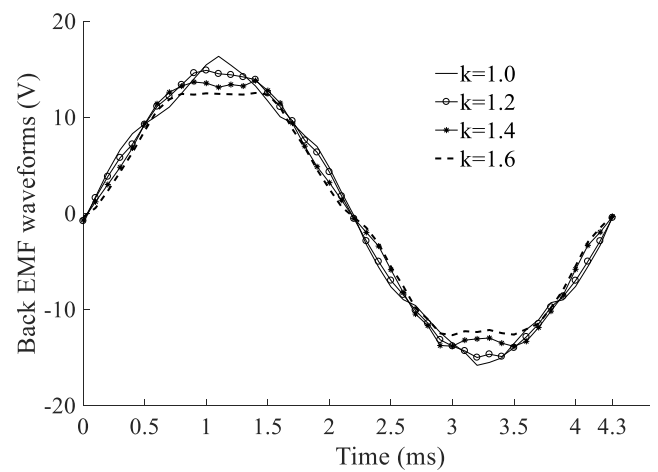
$$T_r = k * T_s \quad (1)$$

where k is the pole-arc coefficient. Then, Fig. 4(b) shows the back EMF waveforms with different pole-arc coefficient k , where the k is varied from 1.0 to 1.6. From Fig. 4(b), it can be seen that only when the pole-arc coefficient $k = 1.2$, the corresponding back EMF waveform is closest to sinusoidal. The detailed harmonic analysis of Fig. 4(b) is shown in Table 1. Moreover, the minimum amplitude of cogging force of FSPMM machine also occurs when the pole-arc coefficient $k = 1.2$, as shown in Fig. 4(c).

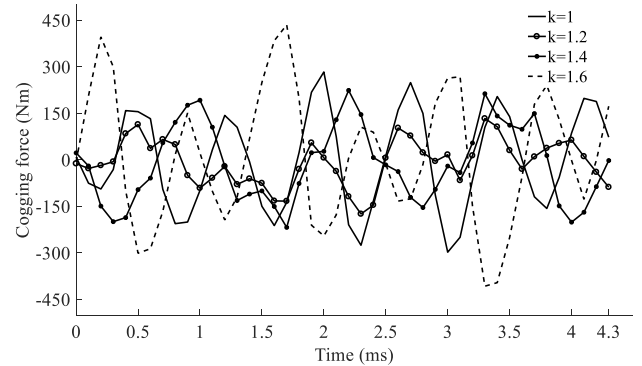
Based on the first step of pole-arc optimization ($k = 1.2$), the skewed slot optimization of rotor is applied in the FSPMM machine. For the straight slot type rotor of FSPMM machine, if divide the mechanical rotating degree θ into N equal parts, and simultaneously calculate the straight slot type back EMF with different mechanical rotating degree $0, \theta/N, 2\theta/N, \dots, \theta$, then the relationship between skewed slot type back EMF and straight slot type back



(a) Tooth width of stator and rotor.



(b) Back EMF waveform.



(c) Cogging force (1000r/min).

FIGURE 4. Pole-arc optimization of FSPMM machine.

EMF can be written as

$$e_{sk}(\theta) = \frac{1}{N+1} \left(\sum_{k=0}^N e_{st}(\theta_k) \right) \quad (2)$$

where $e_{sk}(\theta)$ is the skewed slot type back EMF, $e_{st}(\theta_k)$ is the straight slot type back EMF, and $\theta_k = k\theta/N$.

Fig. 5(a) shows the skewed slot structure of rotor, and the skewed degree is expressed by mechanical angle. Fig. 5(b) shows the back EMF waveforms comparison between

TABLE 1. Harmonic analysis of back EMF waveform of Fig. 4(b).

Normalization of harmonic	k=1	k=1.2	k=1.4	k=1.6
1 th	0.62%	0.56%	0.42%	0.58%
2 th	0.13%	0.10%	0.10%	0.33%
3 th	0.58%	0.63%	0.27%	0.21%
4 th	6.42%	0.77%	6.48%	7.53%
5 th	0.38%	0.57%	0.34%	0.18%
6 th	0.73%	1.18%	0.99%	0.61%
7 th	0.61%	0.58%	0.59%	0.30%
8 th	0.39%	0.41%	0.31%	0.25%
9 th	0.31%	0.47%	1.05%	1.08%
10 th	0.79%	0.33%	0.59%	0.58%
11 th	0.24%	0.71%	0.78%	0.11%
Total harmonic distortion (THD)	11.18%	6.31%	11.92%	11.76%

TABLE 2. Harmonic analysis of back EMF waveform of Fig. 5(b).

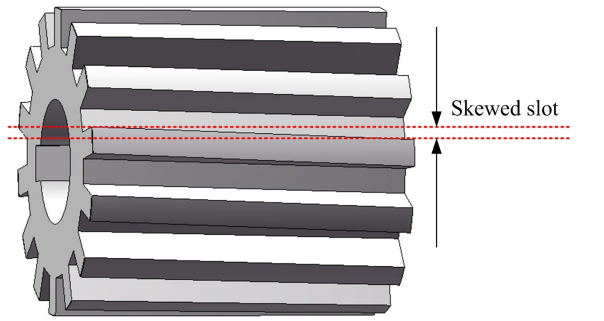
Normalization of harmonic	k=1.2	Skewed slot 3°	Skewed slot 5°	Skewed slot 7°
1 th	0.56%	0.71%	0.79%	0.76%
2 th	0.10%	0.43%	0.33%	0.21%
3 th	0.63%	0.26%	0.09%	0.22%
4 th	0.77%	1.37%	0.04%	0.71%
5 th	0.57%	0.05%	0.08%	0.13%
6 th	1.18%	0.16%	0.15%	0.08%
7 th	0.58%	0.05%	0.08%	0.07%
8 th	0.41%	0.03%	0.14%	0.17%
9 th	0.47%	0.12%	0.08%	0.15%
10 th	0.33%	0.04%	0.08%	0.09%
11 th	0.71%	0.09%	0.05%	0.09%
Total harmonic distortion (THD)	6.31%	3.30%	1.91%	2.68%

pole-arc optimization ($k = 1.2$) and skewed slot optimization, where the skewed slot degree is 5° . From Fig. 5(b), it can be seen that the sinusoidal degree of back EMF waveform can be further improved by the skewed slot optimization of rotor, and the harmonic analysis is shown in Table 2.

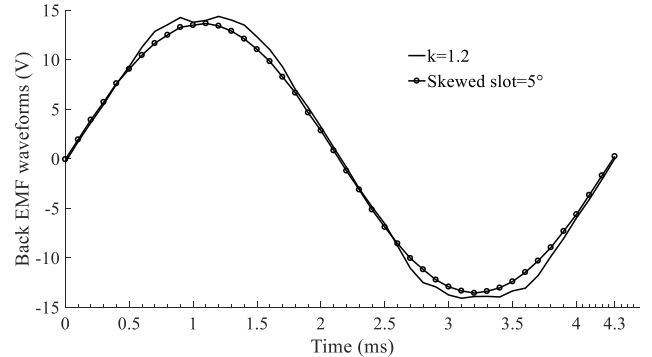
There are two bright points hidden in Table 2 and Fig. 5(c). The first bright point is that there is a suitable skewed slot degree to decrease the harmonic contents of back EMF waveform, and the suitable skewed slot degree is 5° (shown in Table 2). Another bright point is that after the pole-arc coefficient optimization ($k = 1.2$), the cogging force can be further decreased by increasing the skewed slot degree. Besides, the more skewed slot degree, the smaller amplitude of EMF. Therefore, we chose 5 degree of skewed slot as the final parameters for FSPMM machine optimization.

B. HARMONIC ANALYSIS OF BACK EMF WAVEFORM

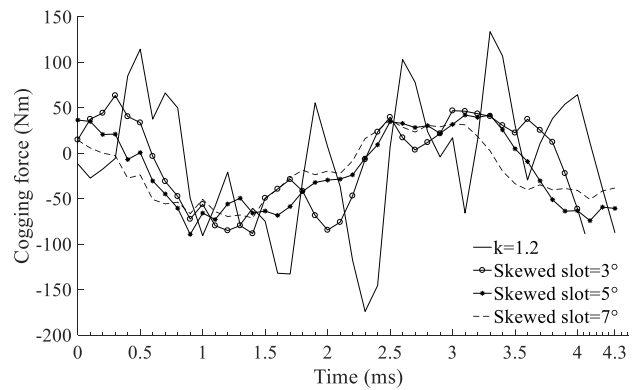
Based on the magnetization of permanent magnet LNG52 (seen the part C of Section II), the flux regulation of FSPMM machine is simulated by numerical analysis software. Fig. 6(a) shows the enhance flux process of FSPMM



(a) The skewed slot structure of rotor.



(b) Back EMF waveform.

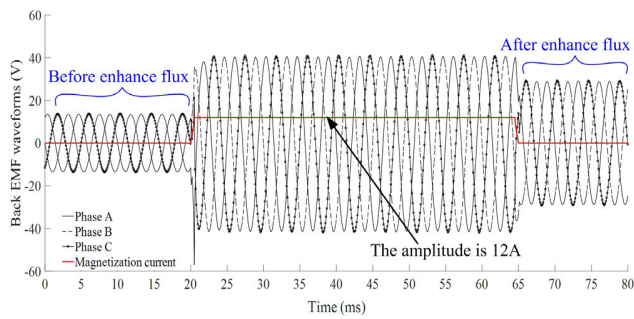


(c) Cogging force.

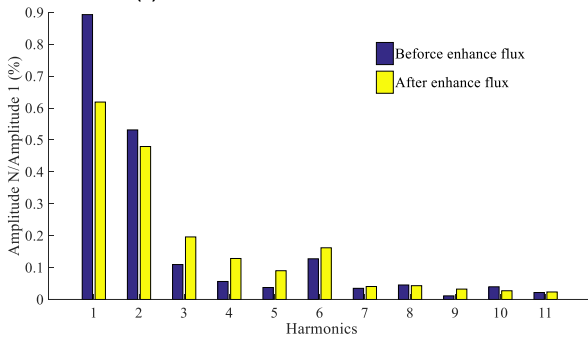
FIGURE 5. Skewed slot optimization of FSPMM machine.

machine by magnetization pulse current, and the skewed slot angle of FSPMM is 5° . As the magnetization direction of LNG52 in Fig. 2, after a magnetization pulse current (12A in Fig. 6(a)), the flux intensity of LNG52 that points the external diameter or internal diameter is weakened, thus air-gap flux density between stator and rotor is increased, and the amplitude of phase back EMF waveform is enhanced (shown in Fig. 6(a)). If the amplitude of magnetization pulse current large enough, than the magnetization direction of LNG52 can be reversed, thus the amplitude of phase back EMF waveform can be further increased. The weaken flux process of FSPMM machine will be elaborated in the experimental section.

Fig. 6(b) illustrates the harmonic analysis of back EMF waveform. Before and after the enhance flux, the THD of back EMF waveform (1st to 11th harmonics) are 1.91% and 1.84% respectively, which is around the THD of skewed slot optimization results (1.91% in Table 2).



(a) Enhance flux of FSPMM machine.



(b) Harmonic analysis of FSPMM machine.

FIGURE 6. Enhance flux and harmonic analysis of FSPMM machine.

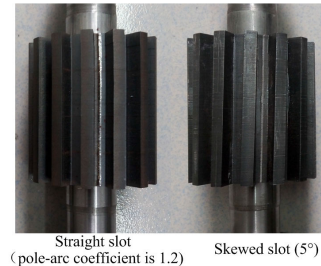
Besides, during the magnetization current process of LNG52, the air-gap flux density is increased, thus the amplitude of cogging force between rotor and stator is also increased. Therefore, the cogging force fluctuate during magnetization current process is another focus that need to be researched in future.

IV. EXPERIMENTAL VALIDATION

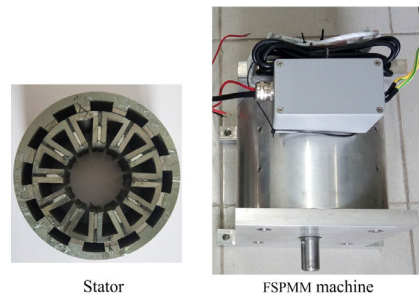
After the optimization of FSPMM machine, a prototype with 12 stator slots and 14 rotor poles is constructed and experimented, as shown in Fig. 7, and the parameters of FSPMM machine is illustrated in Table 3. Fig. 7(a) shows the rotor of FSPMM machine, the pole-arc coefficient of straight slot and degree of skewed slot are 1.2 and 5° respectively. Fig. 7(b) shows the stator structure and prototype, Fig. 7(c) shows the test rig, and Fig. 7(d) illustrates the diagram of magnetization/demagnetization system for LNG52. In Fig. 7(d), the magnetization time is decided by the pulse width of micro control system. Exchanging the positive and negative connection of DC power, the demagnetization process for LNG52 can be achieved.

Fig. 8 shows phase back EMF waveforms of FSPMM machine, the speed is 1000r/min. From the comparison between Fig. 8(a) and Fig. 8(b), it can be seen that the back EMF waveform of skewed slot is more sinusoidal than the straight slot's, which agrees with the harmonics analysis results of Part A of Section 3 (Table 2). The harmonic analysis of Fig. 8(a) and Fig. 8(b) are illustrated in Table 4, the tool of harmonic analysis is Matlab/Simulink.

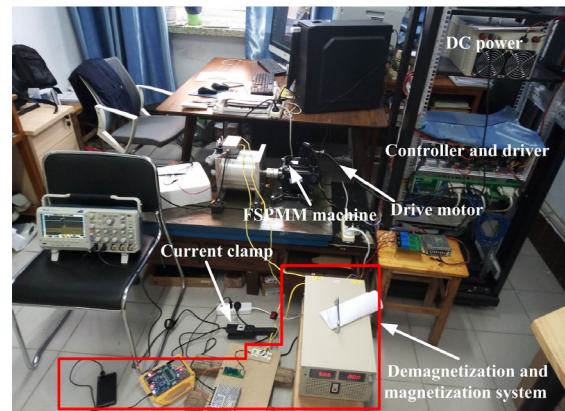
Fig. 9 shows the enhance flux and weaken flux of FSPMM machine, the speed is also 1000r/min. In Fig. 9(a), the magnetization pulse current can reduce the flux intensity



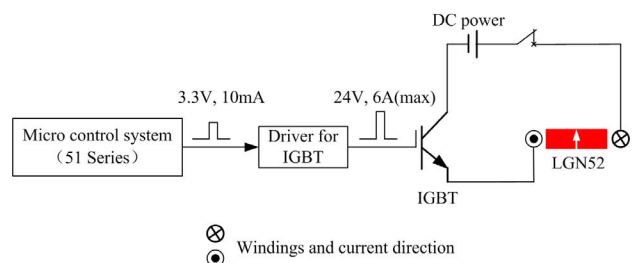
(a) Rotor of FSPMM machine.



(b) Stator and prototype.



(c) Test rig.



(d) Diagram of magnetization and demagnetization system

FIGURE 7. Prototype and experimental of FSPMM machine.

of LNG52, which leads to increase the air-gap flux density between stator and rotor (shown in Fig.2(a)), thus the amplitude of back EMF waveform of FSPMM machine is increased. Fig. 9(b) shows the harmonics analysis of back EMF waveform before enhance flux and after enhance flux, and the THD of before enhance flux and after enhance flux are 2.0% and 2.39% respectively, which agree with the simulation results.

Compared with the magnetization pulse current process of simulation of Fig. 6(a), it can be find that the difference

TABLE 3. The parameters of FSPMM machine.

Specifications	FSPMM machine
Stator outer radius (mm)	79.2
Stator inner radius (mm)	35
Stator	
Stator tooth width (deg.)	8.22
Axial length of stator (mm)	75
Number of stator slots	12
Rotor	
Rotor outer radius (mm)	34.5
Rotor tooth width (deg.)	10
Axial length of stator (mm)	75
Number of rotor poles	14
NdFeB35 thick (mm)	3.5
Permanent magnet	
NdFeB35 length (mm)	15
LNG52 length (deg.)	12
LNG52 thick (mm)	5
Air-gap length (mm)	0.5
Turns of armature winding per phase	140
Others	
Turns of field regulating winding per LNG52	60
Phase number	3
Core of stator and rotor	DW360 50

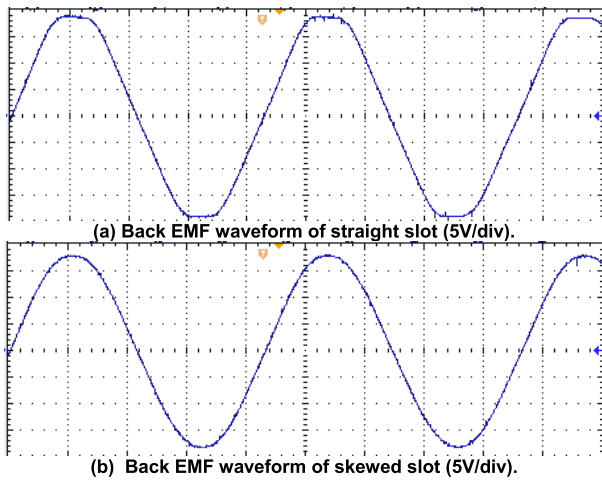


FIGURE 8. The back EMF waveform of FSPMM machine.

TABLE 4. Harmonic analysis of back EMF waveform.

Normalization of harmonic	Straight slot (Fig. 8(a))	Skewed slot (Fig. 8(b))
1 th	1.31%	0.79%
2 th	0.89%	0.33%
3 th	0.61%	0.21%
4 th	1.35%	0.04%
5 th	0.35%	0.08%
6 th	0.92%	0.15%
7 th	0.58%	0.08%
8 th	0.41%	0.14%
9 th	0.47%	0.08%
10 th	0.33%	0.08%
11 th	0.71%	0.05%
Total harmonic distortion (THD)	7.93%	2.03%

occurs in the magnetization pulse current process of experimental (see the red circle part in Fig. 9(a)). Actually, the

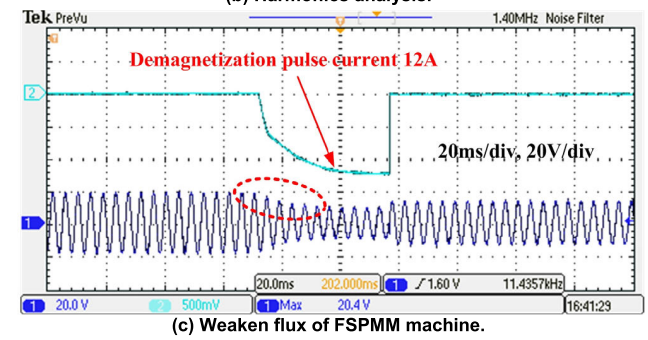
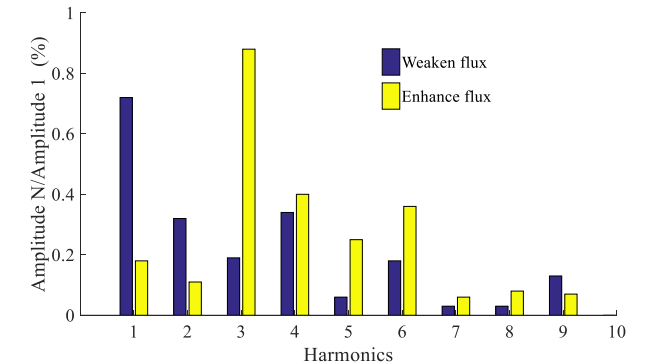
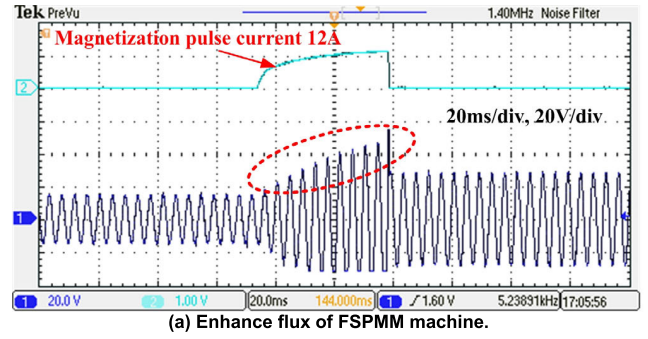


FIGURE 9. Flux regulation and harmonics analysis of FSPMM machine.

increasing processes of magnetization pulse current and back EMF waveforms in Fig. 9(a) is caused by the inductance effect of flux regulating windings, but the inductance effect is not considered in simulation process.

Similarly, if changes the direction of pulse current, then the amplitude of back EMF waveform of FSPMM machine decreases, as shown in Fig. 9(c).

Besides, from Fig. 9(a), it can be known that the amplitude of back EMF waveforms during the magnetization pulse current process is maximum, this means the magnetic flux density of FSPMM machine is also maximum in the magnetization pulse current process. From Fig. 9(c), it can be obtained that the magnetic flux density of FSPMM machine is minimum in the process of demagnetization pulse current.

V. CONCLUSION

The simulation results indicate that after the pole-arc optimization, the back EMF waveform of FSPMM machine can be further sinusoidal by the skewed slot optimization of rotor. Besides, the harmonic analysis show that the THD of back EMF waveforms before and after enhance flux are almost

equal, which is benefit for the control of FSPMM machine by the same method. Then, a FSPMM machine with straight slot and skewed slot is constructed, and the simulation and analysis results are verified by the experimental tests. The simulation and experimental results may be benefit for the research of operational control, flux regulation and industry application of FSPMM machine in future.

In future, the speed range, torque range, operation fluctuation and efficiency of FSPMM machine will be researched, which can indicates the performance of FSPMM machine.

REFERENCES

- [1] Y. Zheng, L. Wu, Y. Fang, X. Huang, and Q. Lu, "A hybrid interior permanent magnet variable flux memory machine using two-part rotor," *IEEE Trans. Magn.*, vol. 55, no. 7, pp. 1–8, Jul. 2019.
- [2] L. Yan-Yan *et al.*, "Design and analysis of novel multi-tooth switched flux permanent magnet memory machine," *J. Mech. Elect. Eng.*, vol. 36, no. 10, pp. 1099–1104, 2019.
- [3] N. Li, X. Fu, J. Zhu, M. Lin, G. Yang, Y. Kong, and L. Hao, "Hybrid-excited series permanent magnet axial field flux switching memory machine," *IEEE Trans. Appl. Supercond.*, vol. 29, no. 2, pp. 1–5, Mar. 2019.
- [4] Q. Wang and S. Niu, "Electromagnetic design and analysis of a novel fault-tolerant flux-modulated memory machine," *Energies*, vol. 8, no. 8, pp. 8069–8085, Aug. 2015.
- [5] D. Wu, T. Sasaki, R. Deodhar, Z. Q. Zhu, A. Pride, and X. Liu, "Switched flux hybrid magnet memory machine," *IET Electr. Power Appl.*, vol. 9, no. 2, pp. 160–170, Feb. 2015.
- [6] H. Yang, X. Chen, H. Lin, Z. Q. Zhu, and S. Lyu, "On-load demagnetization effect of high-coercive-force PMs in switched flux hybrid magnet memory machine," *AIP Adv.*, vol. 9, no. 12, Dec. 2019, Art. no. 125152.
- [7] R. Jayarajan, N. Fernando, and I. U. Nutkani, "A review on variable flux machine technology: Topologies, control strategies and magnetic materials," *IEEE Access*, vol. 7, pp. 70141–70156, 2019.
- [8] W. Wang, H. Lin, H. Yang, W. Liu, and S. Lyu, "Second-order sliding mode-based direct torque control of variable-flux memory machine," *IEEE Access*, vol. 8, pp. 34981–34992, 2020.
- [9] A. Athavale, K. Sasaki, B. S. Gagas, T. Kato, and R. D. Lorenz, "Variable flux permanent magnet synchronous machine (VF-PMSM) design methodologies to meet electric vehicle traction requirements with reduced losses," *IEEE Trans. Ind. Appl.*, vol. 53, no. 5, pp. 4318–4326, Sep. 2017.
- [10] J. H. Cole, M. A. Al-Othman, and O. Wasynczuk, "Hierarchically partitioned finite-element analysis of rotating electrical machinery," *IEEE Trans. Energy Convers.*, vol. 30, no. 1, pp. 1–10, Mar. 2015.
- [11] R. Antonello, L. Ortombina, F. Tinazzi, and M. Zigliotto, "Enhanced low-speed operations for sensorless anisotropic PM synchronous motor drives by a modified back-EMF observer," *IEEE Trans. Ind. Electron.*, vol. 65, no. 4, pp. 3069–3076, Apr. 2018.
- [12] A. Tessorolo, M. Bortolozzi, and C. Bruzzese, "Explicit torque and back EMF expressions for slotless surface permanent magnet machines with different magnetization patterns," *IEEE Trans. Magn.*, vol. 52, no. 8, pp. 1–15, Aug. 2016.
- [13] H. Yang, Z. Q. Zhu, H. Lin, D. Wu, H. Hua, S. Fang, and Y.-K. Huang, "Novel high-performance switched flux hybrid magnet memory machines with reduced rare-Earth magnets," *IEEE Trans. Ind. Appl.*, vol. 52, no. 5, pp. 3901–3915, Sep. 2016.
- [14] M. M. Reza and R. K. Srivastava, "Semi-analytical model for skewed magnet axial flux machine," *Prog. Electromagn. Res. M*, vol. 69, pp. 109–117, May 2018.
- [15] Z. Zhang, C. Xia, H. Wang, and T. Shi, "Analytical field calculation and analysis of surface inset permanent magnet machines with high saliency ratio," *IEEE Trans. Magn.*, vol. 52, no. 12, pp. 1–12, Dec. 2016.
- [16] R. Mirzahosseini, A. Darabi, and M. Assili, "Magnet shifting for back EMF improvement and torque ripple reduction of a TORUS-type non-slotted axial flux permanent magnet machine," *Int. Trans. Electr. Energy Syst.*, vol. 30, no. 4, Apr. 2020, Art. no. e12293.
- [17] G. Yang, X. Fu, M. Lin, N. Li, and H. Li, "Comparative study of flux regulation methods for hybrid permanent magnet axial field flux-switching memory machines," *J. Power Electron.*, vol. 19, no. 1, pp. 158–167, 2019.
- [18] S. Neethu, S. P. Nikam, S. Singh, S. Pal, A. K. Wankhede, and B. G. Fernandes, "High-speed coreless axial-flux permanent-magnet motor with printed circuit board winding," *IEEE Trans. Ind. Appl.*, vol. 55, no. 2, pp. 1954–1962, Mar. 2019.
- [19] W. Hua, M. Cheng, Z. Q. Zhu, and D. Howe, "Analysis and optimization of back EMF waveform of a flux-switching permanent magnet motor," *IEEE Trans. Energy Convers.*, vol. 23, no. 3, pp. 727–733, Sep. 2008.



ZHONGXIAN CHEN received the B.Sc. degree in electronic engineering from the Zhengzhou University of Light Industry, Zhengzhou, China, in 2007, and the Ph.D. degree in electronic engineering from Southeast University, Nanjing, China, in 2015.

He is currently a Lecturer of electronic engineering with Huanghuai University, China. His research interests include permanent magnet motor design and control



YINGJIE CUI received the master's degree in Internet of things from the University of Mysore, Mysore, India, in 2017. He is currently a Lecturer with Huanghuai University, China. His research interests include numerical simulation and data analysis.

• • •